Three-dimensional reconstruction and phenotypic identification of the wheat plant using RealSense D455 sensor

Ming Li[1], Wanteng Zhang[1], Weiting Pan[1], Junke Zhu[2], Xubin Song[1], Chunying Wang[1,3], Ping Liu[1,3*]

(1. *Shandong Engineering Research Center of Agricultural Equipment Intelligentization, Shandong Key Laboratory of Intelligent Production Technology and Equipment for Facility Horticulture, College of Mechanical and Electronic Engineering, Shandong Agricultural University, Tai'an 271018, Shandong, China*;
2. *School of Agricultural Engineering and Food Science, Shandong University of Technology, Zibo 255100, Shandong, China*;
3. *State Key Laboratory of Wheat Improvement, Shandong Agricultural University, Tai'an 271018, Shandong, China*)

Abstract: Accurate and rapid wheat morphology reconstruction and trait collection are essential for selecting varieties, scientific cultivation, and precise management. A single perspective is limited by environmental obstructions, hindering the collection of high-throughput phenotype data for wheat plants. Therefore, a rapid reconstruction method of multi-view three-dimensional point cloud is proposed to realize the high-throughput and accurate identification of wheat phenotype. Firstly, taking wheat at the tillering stage as the experimental object, a multi-view acquisition system based on a RealSense sensor was constructed, and the point cloud data of wheat were obtained from 16 views. Secondly, a joint photometric and geometric objective was optimized, and space location was registered by colored Point Cloud Registration (colored) and Iterative Closest Point (ICP) algorithms. Furthermore, the Multiple View Stereo (MVS) algorithm was used to combine the depth image, RGB image, and spatial position obtained by coarse registration to enable the fine registration of multi-viewpoint clouds. Compared with the traditional Structure From Motion (SFM)-MVS algorithm, our proposed method is much faster, with an average reconstruction time of 33.82 s. Moreover, the wheat plant height, leaf length, leaf width, leaf area, and leaf angle of wheat were calculated based on the three-dimensional point cloud of the wheat plant. The experimental results showed that the determination coefficients of the method are 0.996, 0.958, 0.956, 0.984, and 0.849, respectively. Finally, phenotypic information such as compact degree, convex hull volume, and average leaf area of different wheat varieties was analyzed and identified, proving that the method could capture the phenotypic differences between varieties and individuals. The proposed method provides a rapid approach to quantify wheat phenotypic traits, aiding breeding, scientific cultivation, and environmental management.

Keywords: wheat plant, RealSense sensor, MVS, three-dimensional point cloud, phenotypic traits
DOI: 10.25165/j.ijabe.20251804.9169

Citation: Li M, Zhang W T, Pan W T, Zhu J K, Song X B, Wang C Y, et al. Three-dimensional reconstruction and phenotypic identification of the wheat plant using RealSense D455 sensor. Int J Agric & Biol Eng, 2025; 18(4): 254–265.

1 Introduction

Research on wheat phenotypes is essential for breeding high-yielding, high-quality, and resilient varieties[1,2]. The height and leaf area of the wheat plant reflect the growth rate and robustness of the plant, and the leaves have an important influence on wheat yield and disease resistance[3,4]. However, the cost of manually studying wheat phenotypic information is enormous, and it is prone to error and takes a long time. Addressing these problems is critical to accelerate the breeding process and optimize field management[5]. With the development of modern science and technology, especially the development of sensor technology and computer vision technology, it is possible to obtain crop morphological characteristics information utilizing high throughput, high precision, and high automation[6].

At present, two-dimensional images and three-dimensional point clouds are widely used to obtain plant phenotypes. Among them, much progress has been made in obtaining one-dimensional and two-dimensional phenotypic indicators based on two-dimensional images[7-10], but the accuracy of phenotypic indices obtained under the condition of severe occlusion and complex plant-type structure is poor[11], and three-dimensional phenotypic information is missing. To overcome the dimensional data loss, researchers proposed a three-dimensional point cloud approach. Kargar et al.[12] used mobile lidar to reconstruct three-dimensional point clouds of agricultural sample plots and accurately measured leaf area. Sun et al.[13] analyzed the high-throughput phenotype of cotton fields and the growth status of cotton plants by three-dimensional reconstruction of cotton fields with lidar. Lidar had excellent point cloud acquisition performance and showed strong advantages in plant phenotype evaluation, but its long scanning time and high equipment price made it difficult to be widely applied in the agricultural field[14–16]. Pound et al.[17] collected multi-view images of wheat plants with RGB cameras. Westoby et al.[18] obtained

Received date: 2024-06-23 **Accepted date:** 2025-05-12
Biographies: Ming Li, MS, research interest: crop phenotyping robots, Email: crazyliming@163.com; **Wanteng Zhang**, MS, research interest: 3D reconstruction and segmentation algorithm of wheat, Email: zwt2685235672@163.com; **Weiting Pan**, MS, research interest: 3D reconstruction and segmentation algorithm of wheat, Email: 17861501669@163.com; **Junke Zhu**, Professor, research interest: wheat breeding, Email: zhunjunke@sdut.edu.cn; **Xubin Song**, PhD, research interest: computer vision for crop phenotyping, Email: 2021110415@sdau.edu.cn; **Chunying Wang**, Professor, research interest: image processing for wheat phenotyping, Email: wcychunying@126.com.
***Corresponding author: Ping Liu**, Professor, research interest: key technology of crop phenotyping robots. College of Mechanical and Electronic Engineering, Shandong Agricultural University, Tai'an 271018, Shandong, China. Email: liupingsdau@126.com.

camera pose and sparse point cloud by SFM algorithm. Furukawa and Hernández[19] estimated depth by MVS algorithm, built dense point cloud generation by matching views, reconstructed the three-dimensional model of wheat plants, and extracted their phenotypic measurements. Wu et al. also used the same method to reconstruct the wheat plant model and designed different multi-view image acquisition devices[20,21]. The reconstruction method has the advantages of low cost, wide application conditions, and high accuracy of the wheat three-dimensional model. However, it needs to estimate the image depth in the reconstruction process, which costs a lot of time and leads to slow reconstruction speed[22,23]. In contrast, the RealSense D455 sensor based on the principle of structured light can directly obtain color images and depth information, making up for the problem that the MVS algorithm takes a long time to estimate the depth. It is portable, inexpensive, and easy to integrate into equipment including Low Earth orbit platforms and autonomous land and air vehicles[24].

Therefore, a multi-view acquisition system based on the RealSense D455 depth camera was constructed in this study to derive RGB image and depth image data of a single wheat plant. The RGB image and depth image of wheat were fused to obtain the point cloud, and a high-throughput method for automatic and rapid identification of wheat phenotypic traits was proposed. Firstly, a joint photometric and geometric objective was optimized, and the spatial location was registered using a combination of colored Point Cloud Registration (colored) and Iterative Closest Point (ICP) algorithms. Then, combined with the obtained spatial position, RGB image, and depth image, the MVS algorithm was used to match the views, and a complete and reproducible three-dimensional point cloud model of a single wheat plant was generated. The phenotype characteristics of wheat were calculated and extracted based on the three-dimensional point cloud model to meet the actual needs of wheat with high yield, high quality, and strong stress resistance.

2 Materials and data collection

2.1 Experimental materials

In this study, based on the identification of wheat phenotype and screening of high-quality wheat varieties, a method for rapid phenotypic identification of trait information was designed. Wheat was cultivated in planters to demonstrate high-throughput methods for sensing varietal and phenotype characteristics. The wheat was grown in the growth chamber in the State Key Laboratory of Wheat Improvement in Shandong Agricultural University. The room temperature of the growth chamber was maintained at 23°C, the air humidity was maintained at 40%, and the photoperiod was 16 h provided. Light illumination in the chamber was 30 000 lx. The plants were placed in 5.7 L pots with the PINDSTRUP peat soil. The pH of the soil source ranges from 5.5-6.5, mixed with a certain proportion of vermiculite and perlite.

The tillering stage of wheat is the main stage that determines the spike number per unit area[25]. In the experiment, point cloud data, image information, and phenotype data were obtained from the tillering stage of wheat. To assess the applicability of the algorithm proposed in the study, three varieties of wheat - QiMin8, ShanNong17, and BaiNong58 - with significant differences in leaf compactness, leaf morphology, and tillering ability, were selected for the experiment. QiMin8 (QM) has wide and long leaves, dark green color, strong tillering ability, and loose plant shape. ShanNong17 (SN) has strong tillering ability, slightly loose plant shape, upswept flag leaf, and long spike, and BaiNong58 (BN) is a dwarf-resistant variety, with strong tillering ability, compact plant shape, and wide flag leaf. Samples were taken at the tillering stage of wheat on October 5, October 15, October 25, and November 5, 2022 (three duplicates for each variety). The detailed measured tiller numbers of each sampled shoot are listed in Table 1. Each cultivar involves three sample replicates.

Table 1 Tiller numbers of each sampled wheat ear shoot in 4 d

Variety	QM			SN			BN		
ID	1	2	3	1	2	3	1	2	3
2022.10.05	5	6	6	7	6	6	7	7	5
2022.10.15	7	8	9	9	7	7	7	7	6
2022.10.25	8	8	8	10	8	9	8	7	6
2022.11.05	7	6	6	7	7	6	6	5	5

The basic computer configuration for processing 3D point cloud data is with a Core i5-10200 CPU, 4.0 GB RAM, and NVIDIA GeForce GTX 1650 graphics card, as well as a solid-state hard disk of Micron MTFDHBA256TDV.

2.2 Experiment process

The three-dimensional reconstruction of wheat plants and acquisition of phenotypic traits were based on the experimental design depicted in Figure 1.

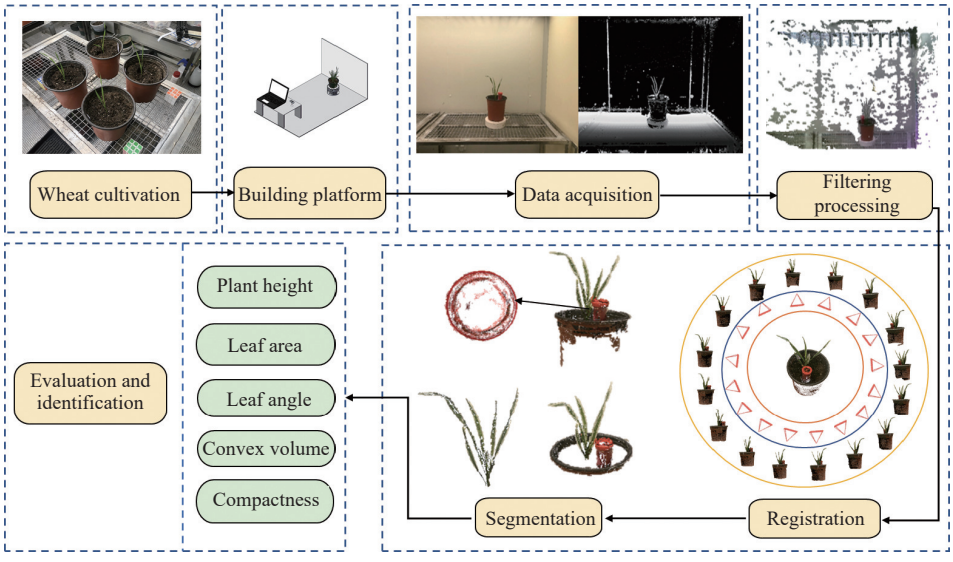

Figure 1 Flow chart of data processing

Firstly, a data acquisition platform was created using the RealSense D455 sensor to capture point cloud data with color information for the target crop.

Secondly, conditional filtering and Statistical Outlier Removal (SOR) filtering were applied to extract the wheat plant from the original point cloud data.

Thirdly, the wheat point clouds were registered and fused using colored-ICP and the MVS algorithm along with depth maps.

Fourthly, the Alpha Shape method was employed to accurately define the wheat plant's boundary, after which phenotypic traits such as plant height, leaf area, leaf angle, shoot convex volume, and compactness were calculated.

Finally, the accuracy of the three-dimensional model and the computational outcomes of the wheat plant phenotypes were dissected, evaluated, and identified.

2.3 Multi-view data acquisition

The multi-view image acquisition platform was built in an indoor environment, and the light source was the LED light below the ceiling of the growth chamber. During the operation of the platform, the wheat plant was evenly illuminated and would not be blocked. The platform consists of a turntable, a shooting device, and a background plate, and the construction of the shooting scene is shown in Figure 2.

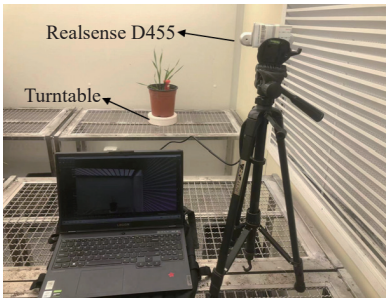

Figure 2 Three-dimensional data synchronous acquisition platform of wheat plant

Among them, the turntable was composed of a turntable unit and a calibration unit. The turntable unit had a built-in rotation motor to drive the wheat plant under test to rotate. The diameter of the turntable was 20 cm, the speed was adjustable, and the calibration unit was 12 cm high. On top of the calibration unit was a red disk with a diameter of 4 cm, which was used as the scale for later point cloud calibration. The shooting unit consisted of a triangle stand, a RealSense D455 sensor, and a high-performance laptop connected to the laptop via a USB cable.The depth collection range was 0.2-10 m. The background plate was white to reduce reconstruction noise.

Accurate color image and depth image information of wheat could be collected by the system in a short time.

2.4 Data acquisition

The wheat plant was located in the center of the turntable. The calibration unit was placed in a pot and the wheat plant was not in contact with the calibration unit. The best distance between the sensor, turntable, and background was that the wheat plant under test and the calibration unit could be fully photographed. To capture the overall structure of the wheat as much as possible, the horizontal distance between the RealSense D455 sensor and the plant turntable was set at 1.5 m. The distance was chosen to obtain information about the inner leaves and stems surrounded by the outer leaves of the wheat. The sensor was placed at a height of 0.9 m and took a top view of the wheat plant. The distance between the turntable and the background plate was 0.3 m.

The lighting environment for multi-angle images was the indoor ordinary LED lighting source. The turntable rotated 22.5 degrees each time for a total of 16 times. The multi-view image acquisition program controlled the acquisition of the RealSense D455 sensor. Each time the turntable rotated, the images were collected once at an interval of 1 s, and the plants rotated for 1 week. A total of 16 multi-view RGB images and 16 depth images were collected. Multi-view data collection was completed within 60 s for each wheat plant, and the images were automatically named and stored. The wheat plant images collected are shown in Figure 3.

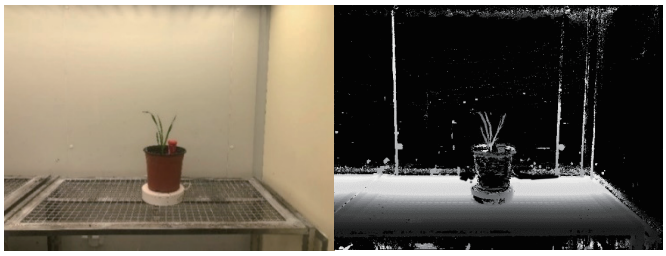

Figure 3 Image acquisition of wheat plant

3 Calculating methods

Point cloud dispersion in three-dimensional space for the wheat plant is irregular, lacking a specific numerical relationship due to its complex three-dimensional canopy morphology. Establishing the spatial relationships between these three-dimensional point clouds is challenging. To create a relationship between the depth and color images of the wheat plant captured by the RealSense D455 sensor, the mapping function of sensor[26] was used. Each point on the wheat plant after image registration contained three-dimensional *x*-*y*-*z* coordinates and RGB color attributes. Additionally, there were undesired backdrop point clouds and some noise in the original images, affecting the space location and three-dimensional structure of the wheat plant. Thus, the preprocessing of three-dimensional point cloud involved two key steps:

Firstly, conditional filtering was applied to eliminate redundant background point cloud, enhancing the significance of the point cloud by focusing on wheat structures.

Secondly, to address outlier issues with the wheat plant's point cloud, the SOR filtering algorithm was employed. This step aimed to improve measurement accuracy and the speed of recognizing wheat plant characteristics.

These preprocessing steps resulted in an accurate point cloud, featuring a clear wheat structure devoid of any clustered outliers or non-matching points.

3.1 Three-dimensional point cloud preprocess

3.1.1 Conditional filter

Three-dimensional point cloud, background noise, and mottled spots of wheat plants were obtained by the RealSense D455 sensor. According to the general attributes of points, conditional filtering was used to eliminate these points. The target plant point cloud was obtained from the primary point cloud of a single view by using the condition constraint of coordinate execution in Equation (1):

$$\begin{aligned} X_d < x < X_u \\ Y_d < y < Y_u \\ Z_d < z < Z_u \end{aligned} \quad (1)$$

where, (X_d, X_u), (Y_d, Y_u), and (Z_d, Z_u) represent the limited range of three-dimensional Cartesian coordinates. Since the RealSense

sensor is stationary, the same constraints are applied to the point clouds of each view. The clear wheat plant's point cloud was obtained as shown in Figure 4.

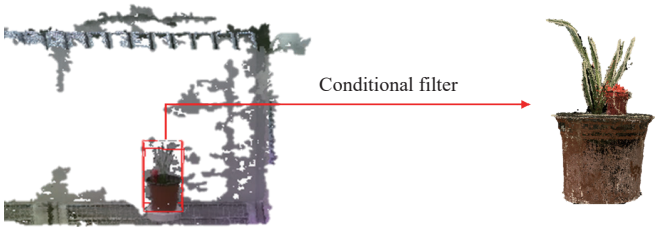

Figure 4 Point cloud after conditional filter

The wheat plant point cloud retained substantial proximal noise and anomalies near leaf structures. The SOR algorithm was applied to streamline point cloud data by eliminating spatially dispersed noise artifacts.

3.1.2 SOR filter

Point clouds representing wheat plants often exhibited uneven spacing, resulting in numerous sparse outliers. Any point within leaf-space held valuable information, with denser regions conveying more information. On the contrary, noisy or outlier points were seen as less informative and typically had a larger average point-to-point distance within the point cloud. Considering these conditions, the information expressed by points where the average distance to their neighboring points within the point cloud exceeded a specific threshold was disregarded[27,28].

The SOR filtering involves analyzing each point's k neighborhood statistically and calculating the mean distance from the point to the k-neighbor. The filter operates under the assumption that the distances follow a Gaussian normal distribution. Points with an average distance outside the predefined threshold are identified as outliers and subsequently removed from the dataset. The steps of the process are as follows:

(1) Calculate the distance d_i from each point to its k-neighbors.

$$d_i = \sqrt{(x_0 - x_i)^2 + (y_0 - y_i)^2 + (z_0 - z_i)^2} \tag{2}$$

(2) Calculate the sum D of d_i and mean distance μ between any point and its nearest k-neighbors.

(3) Geometry is determined by μ and standard deviation σ, that is, as in the following equation with Gaussian distribution:

$$\sigma = \sqrt{\frac{\sum_{i=1}^{k}(d_i - \mu)}{k}} \tag{3}$$

4) d_t is considered as the distance threshold, as in the following equation. Points with μ greater than d_t are rejected.

$$d_t = \mu + n \cdot \sigma \tag{4}$$

where, n is the arithmetic-coefficient of the standard deviation of the distance. The filter outcomes are shown in Figure 5.

Figure 5 Point cloud after SOR filter

The point clouds of wheat plants with 16 views after filtering are shown in Figure 6.

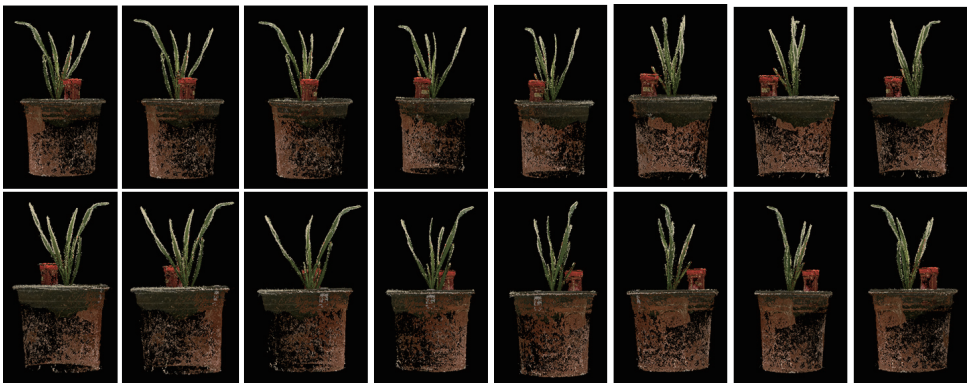

Figure 6 Point clouds of wheat plants from 16 views after filtering

3.2 Three-dimensional point cloud registration from multiple views

To perform precise registration of multi-view point clouds, the colored-ICP algorithm was employed in this study for optimizing a joint photometric and geometric object to calculate the relative position of the camera and complete the coarse registration. The MVS algorithm was applied to the coarse registration of wheat plant point cloud. The registration process of the multi-view three-dimensional point cloud is shown in Figure 7b.

3.2.1 Colored-ICP algorithm coarse registration

The colored-ICP algorithm jointly optimizes the photometric objective and the point-to-plane ICP objective to register the RGB-D sequence and colored point cloud of wheat plants. Firstly, the RGB-D image sequences are registered to create segments, and then the joint optimization objective is generalized to calculate the camera pose and register the colored point clouds. The wheat plant point clouds from 16 views are shown in Figure 7a.

Figure 7 Registration principle of point cloud

The transformation matrix equation between point clouds is as follows:

$$E(T) = (1-\sigma)E_C(T) + \sigma E_G(T) \quad (5)$$

where, E_C and E_G are the photometric and geometric errors, respectively. $\sigma \in [0, 1]$ is a weight that balances the two terms.

$$E_G(T) = \sum_{(p,q)\in\kappa} ((p - Tq)\cdot n_p)^2 \quad (6)$$

where, κ is the corresponding set in the current iteration; n_p is the normal to point p; E_c is conversion error about color, that is, the difference between the color of the measurement point q (denoted as $C(q)$) and its projected color on the tangent plane of p.

$$E_C(T) = \sum_{(p,q)\in\kappa} (C_p(f(Tq)) - C(q))^2 \quad (7)$$

where, $C_p(f(Tq))$ is a precomputed function defined continuously on the tangent plane of p. The function $(f(Tq))$ projects a three-dimensional point onto the tangent plane.

The markers in the basin have regular shapes and prominent colors. Therefore, the colored-ICP algorithm was used to register the red cylindrical markers in the basin to obtain accurate initial camera poses, as shown in Figure 7b, and coarse registration point cloud, as shown in Figure 7c[29].

3.2.2 MVS algorithm fine registration

The point clouds of wheat plants with multiple views obtained a better initial pose after coarse registration. In order to enable rapid three-dimensional reconstruction, the MVS algorithm was applied for fine registration.

The MVS algorithm is a process that involves finding points in space with luminosity consistency, after obtaining the initial pose of the point cloud from multiple camera views, and performing stereo matching on the scene. The algorithmic process is illustrated in Figure 8: Firstly, a three-dimensional point P was selected from the initial coarse registered point cloud. Then, the three-dimensional points were projected onto the images using the camera's intrinsic and extrinsic parameters. Two small square patches, $\boldsymbol{f}$ and $\boldsymbol{g}$, were extracted with the projection point as the center. The similarity between the scenes contained in these patches was then evaluated. Conversely, if the point lay outside the object, there was a noticeable difference between the two patches. By measuring the consistency between these patches, the algorithm could estimate the likelihood that the three-dimensional point lay on the object's surface.

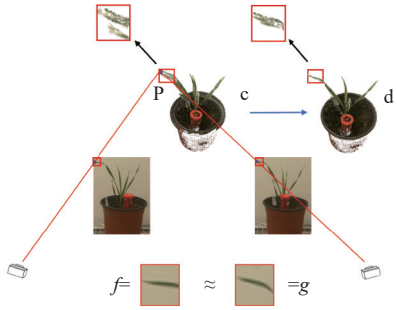

Figure 8 MVS algorithm process

Given a set of N input images and a three-dimensional point p seen by all the images, one can define the photo-consistency of p w.r.t. each pair of images I_i and I_j as:

$$C_{ij}(p) = \rho(I_i(\Omega(\pi_i(p))), I_j(\Omega(\pi_j(p)))) \quad (8)$$

where, $\rho(f, g)$ is a similarity measure that compares two vectors, $\pi_i(p)$ denotes the projection of p into image i, $\Omega(x)$ defines a support domain around point x, and $I_i(x)$ denotes the image intensities sampled within the domain. Every photo consistency measure can be described as a particular choice of ρ and Ω.

The photographic consistency points were found in three-dimensional space, the noise points of coarse registration were removed, and the fine registration of the wheat point cloud was realized.

3.3 Original point cloud preprocess

After obtaining the fine-registered wheat plant point cloud, it is essential to correct the point cloud and the positive orientation of the point cloud to convert it to its real size with the *X*-*O*-*Y* plane as the reference plane and the *Z*-axis as the positive orientation. In addition, wheat plants have to be segmented from the original point cloud to promote the following phenotypic extraction.

The original point cloud of the wheat plant was subjected to coarse segmentation as shown in Figure 9a, and any points with a height less than 40% of the *Z*-axis direction were eliminated. The process yielded the point cloud depicted in Figure 9b. Subsequently, to calibrate the size of the point cloud, markers placed in pots were used as a reference. Next, the border points were identified, and the marker circumference was estimated, as shown in Figure 9c. Finally, the diameter ratio of the approximated circumference to the actual marker plate size was utilized as a scaling factor to calculate the dimensions of the wheat point cloud. Figure 9d shows the segmentation result.

Figure 9 Process of point cloud calibration and shooting segmentation

The obtained results were then compared with manual measurements to evaluate the accuracy of the calibration. To ensure accuracy, multiple measurements were taken and averaged to avoid human error. The error generated between the estimated and actual diameter was quantitatively evaluated using the indicator mean absolute percentage error (MAPE) metric as shown in Equation (9), where $\tilde{d}_i$ is the estimated diameter from the point cloud, and d_i is the real size of the plate (4 cm):

$$\text{MAPE} = 100\% \frac{1}{n} \sum_{i=1}^{n} \frac{|\tilde{d}_i - d_i|}{d_i} \quad (9)$$

3.4 Calculation method of phenotypic traits for the wheat plant

3.4.1 Calculation method of wheat plant height

The difference in height between the maximum and minimum values of the point cloud on the *Z*-axis was recognized as the height of the plant[30].

3.4.2 Calculation method of projected area and multi-layer projected area

The plant point cloud was initially projected onto the *X*-*O*-*Y* plane, as shown in Figure 10b. The sparsely sampled points were used to generate a mesh using the greedy triangulation algorithm. The summation of the triangle mesh areas was recognized as the projected area of the plant, as shown in Figure 10c. The plant point cloud was then divided into equal segments in order to calculate the

multilayer projection area, which was used to determine the projected area of the plant, as shown in Figure 10. Figure 10a and Figure 10d show the initial point cloud of wheat and multi-layer initial point cloud of wheat, respectively. Figure 10e shows the plant point of multi-layer onto the *X*-*O*-*Y* plane. Figure 10f shows the summation of the triangle mesh areas, which was recognized as the multi-storey projected area.

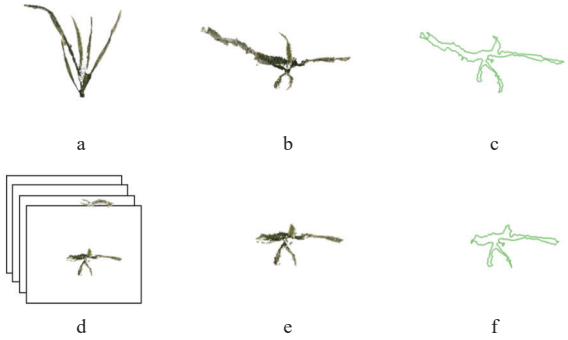

Figure 10 Projected area and multi-storey projected area calculation process

3.4.3 Calculation method of leaf area and leaf angle

Firstly, the wheat plant point cloud (Figure 11a) was downsampled using the voxel-grid to enhance the computational performance of the next phase and to ensure the consistency of the point cloud concentration, as shown in Figure 11b. The leaves were extracted from the wheat plant, as shown in Figure 11c. The point cloud was then smoothed by moving least squares to keep the bending and twisting phases of the blade, as shown in Figure 11c and Figure 11d. Furthermore, the mesh was generated from the smoothed point cloud using greedy triangulation. Finally, the total of the areas of all triangular cross sections was the wheat leaf area. Figure 11e shows the combined visualization of the generated mesh and the original colored point cloud.

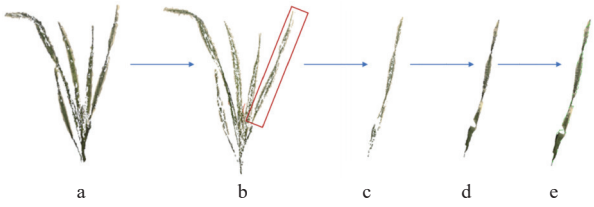

Figure 11 Leaf area estimation

When calculating leaf angle as shown in Figure 12, random point *A* on the main stem of wheat, tillering on wheat, and random endpoint *B* above *A* were linked to form line segment *a*. The vertex *A* was linked to the endpoint *C* on the tillering form segment *c*. Then, the leaf angle θ was calculated from the coordinates of *A*, *B*, and *C* and the lengths of *a*, *b*, and *c*[31].

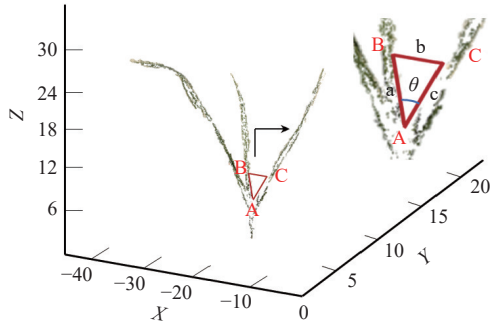

Figure 12 Calculation diagram of leaf angle

3.4.4 Calculation method of wheat plant convex volume and compactness

The convex volume was estimated by calculating the convex hull of the plant point cloud, as shown in Figure 13a. As shown in Figure 13b, the degree of compactness of wheat is the ratio of projected area to convex hull area[32].

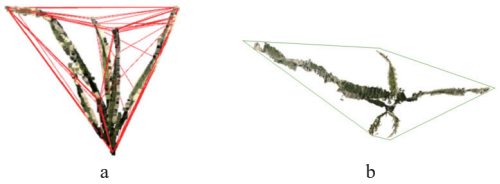

Figure 13 Wheat plant convex volume and compactness calculation

4 Results and discussion

4.1 Analysis of registration results

The object is reconstructed by the MVS algorithm. The reconstruction effect depends on the quality of the input image and camera parameters. To obtain camera parameters, MVS algorithms are often used in combination with SFM algorithms. But SFM algorithm is slow and has low precision in obtaining camera parameters. It can not meet the demand for precision agriculture for virtual plant reconstruction with low time cost and high precision. Therefore, the colored-ICP algorithm is applied to the coarse registration of point clouds to obtain camera parameters accurately and quickly. In addition, the method of using the MVS algorithm combined with depth maps eliminates the process of stereo matching, which saves a lot of time [33].

4.1.1 Analysis of coarse registration performance

The point clouds of each viewpoint after conditional filtering and SOR processing were registered. Colored-ICP algorithm combined with photometric and geometric optimization algorithms was used to calculate the camera pose according to Equation (5). Camera parameters and coarse registration point cloud were obtained. The effect is shown in Figure 14, where the camera pose of each view image was calculated more accurately, and the coarse registration point cloud was relatively complete.

Traditional SFM uses a robust SIFT algorithm to extract feature points in images and uses a nearest neighbor method to match feature points. To ensure the fairness of the comparison between the processing effects of different algorithms, the image of each view was cropped, and the range of cropping was the same as that of the point cloud processed by conditional filtering. The image was cropped and processed as shown in Figure 15.

Figure 14 Effects of colored-ICP coarse registration

Figure 15 Effects of images of each view after cropping

The processing effect of SFM algorithm is shown in Figure 16.

Figure 16 Effects of SFM sparse reconstruction

In Figure 16, the camera pose of each view angle image calculated by the SFM algorithm was basically in front of the wheat plant, which was caused by the fact that the image background was consistent and the wheat plant leaves were slender, making it difficult to capture the feature points of wheat leaves. So, the camera pose calculation was not accurate. As a result, the point cloud obtained by SFM sparse reconstruction was also not complete enough and had poor accuracy.

The time cost and completeness of the reconstructed point cloud of the colored-ICP algorithm and SFM algorithm are compared, as listed in Table 2:

In Table 2, the experiments were repeated four times using the two algorithms, respectively. The average total points of the point cloud obtained by using the colored-ICP algorithm is 31 943, the average number of points after removing the pot and calibration object is 9899, and the average time consumption is 29.1686 s. The average total points of the point cloud obtained by using the SFM algorithm is 9735, the average number of points after removing the pot and calibration object is 2231, and the average time consumption is 36.071 58 s.

Table 2 Time cost and registration accuracy of coarse registration algorithms

Algorithm	Total points	Total points of the wheat plant	Time cost/s
colored-ICP	31 885	9844	29.3503
	32 018	9916	29.7877
	32 114	9907	28.4832
	31 755	9930	29.0532
SFM	9733	2294	35.4650
	9664	2188	36.0872
	9795	2284	36.4358
	9751	2158	36.2983

Therefore, compared with the wheat point cloud reconstructed by the traditional SFM sparse reconstruction, the wheat point cloud obtained by the colored-ICP algorithm for coarse registration has higher completeness and less time consumption.

4.1.2 Analysis of fine registration performance

The registration results of the proposed and the conventional algorithm are shown in Figures 17-19.

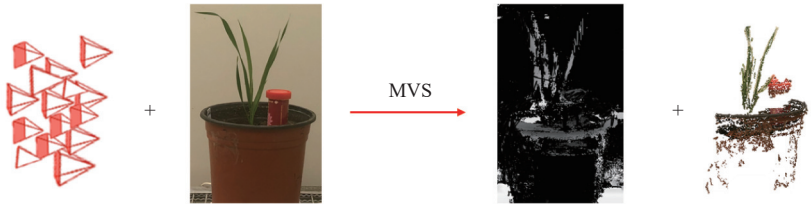

Figure 17 Result of SFM-MVS algorithm

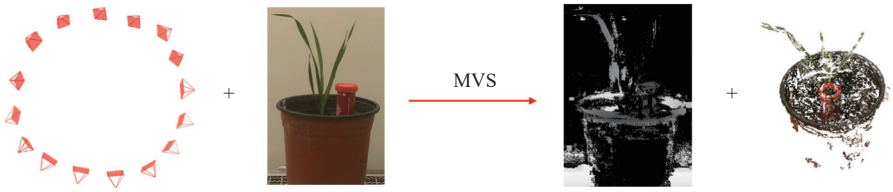

Figure 18 Result of MVS algorithm after colored-ICP algorithm coarse registration

Figure 19 Result of MVS combined with depth map algorithm after colored-ICP algorithm coarse registration

Figure 17 shows the results of SFM-MVS algorithm registration. Figure 18 shows the result of MVS algorithm following colored-ICP algorithm coarse registration. Figure 19 shows the result of MVS combined with the depth map algorithm after the colored-ICP algorithm coarse registration.

In Figure 17, each view RGB image and camera pose are used as input. Due to the inaccuracy of the camera pose obtained by the sparse reconstruction of SFM, the depth map calculated by the MVS algorithm is not accurate enough, and the wheat plant point cloud obtained by the dense reconstruction is incomplete, which affects the computational precision of phenotype characteristics. In addition, the process of obtaining the depth map of the image by using the MVS algorithm for stereo matching also consumes a lot of time.

In Figure 18, RGB images are combined with camera poses calculated by the colored-ICP algorithm. Then the MVS algorithm is used to stereo-match the images of each view to obtain the depth map of each view, and finally the wheat point cloud is reconstructed. There are two problems with this method. Firstly, it will consume a lot of time in the process of computing the depth map. Secondly, the accuracy of the computed depth map is not high, and many pixels are missing depth values, resulting in incomplete wheat point cloud reconstruction with large errors.

In Figure 19, the RGB image and depth image obtained by the RealSense D455 sensor are combined with the camera pose obtained after coarse registration by the colored-ICP algorithm, and MVS algorithm is applied to fine registration, which skips the stereo matching process and saves a lot of time. In addition, the depth image obtained by the RealSense D455 sensor is more accurate, and the final reconstructed wheat point cloud is more complete.

In Figure 19, the proposed method has a clearer three-dimensional wheat plant texture. To further validate the performance of the three-dimensional reconstruction method, time-cost comparative results and registration precision comparative results are listed in Table 3.

Table 3 Time cost and registration accuracy of different inputs and algorithms

Combination number	Coarse registration	Fine registration	Input	Total points	Total points of the wheat plant	Time cost of coarse registration/s	Time cost of fine registration/s	Total time cost/s
1	SFM	MVS	RGB +CAMERA POSE	25 641	6071	36.0872	1466.53	1502.6172
				27 650	6766	38.6647	1531.33	1569.9947
				28 035	7296	39.9635	1619.67	1659.6335
				29 286	7614	41.7587	1699.47	1741.2287
				31 988	8837	43.4985	1771.19	1814.6885
2	colored-ICP	MVS	RGB +CAMERA POSE	31 975	8360	28.4683	1409.67	1438.1383
				32 092	8738	29.0781	1512.32	1541.3981
				35 621	10 647	30.4413	1536.67	1567.1113
				37 145	11 128	30.6411	1654.9	1685.5411
				41 155	12 041	31.4438	1725.61	1757.0538
3	colored-ICP	MVS	RGB+DEPTH +CAMERA POSE	34 589	10 126	28.4683	3.0385	31.5068
				35 602	10 508	29.0781	3.1688	32.2469
				37 308	11 858	30.4413	3.8604	34.3017
				39 424	12 961	30.6411	4.1244	34.7655
				42 942	14 072	31.4438	4.8602	36.304

Combinations 2 and 1 in Table 3 show that the point clouds obtained by registration using the colored-ICP algorithm and MVS algorithm are more complete than those obtained by the SFM-MVS algorithm, and the wheat plant point cloud accounts for a higher proportion, 28.50%, of the total point cloud.

Combination 3 and Combination 2 in Table 3 show that the camera pose obtained by the colored-ICP algorithm is coarsely registered, the RGB images and depth images are used as input, and the point cloud reconstructed by the MVS algorithm is more complete. The wheat plant point cloud accounts for a higher proportion of the total point cloud, which is 31.24%, and the average reconstruction time is 33.82 s. It is 97.89% faster than Combination 2.

Therefore, the proposed method can greatly shorten the reconstruction time while obtaining high-precision camera poses. Under the same conditions, computational performance and registration precision are better than the traditional SFM-MVS algorithm. The reconstructed wheat was more observable and structurally clearer.

4.2 Phenotype characteristic calculation and analysis

4.2.1 Plant height calculation and analysis

In order to validate the validity of reconstruction-based three-dimensional wheat plant height calculation method, the correlations between the calculated values and the measured values were investigated. Plant heights of the reconstructed wheat plant structure model were calculated according to the plant height calculation method presented in Section 3.4.1.

The error of plant height calculation is shown in Figure 20.

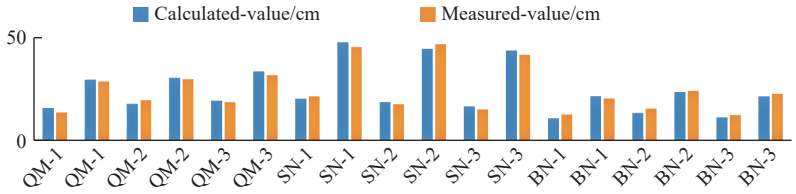

Figure 20 Calculation error of plant height

Figure 20 shows the calculated data's error range (0.1-1.8 cm), average error (0.917 cm), and RMSE (0.424 cm) compared to measured values. The calculation achieved 97.03% accuracy with a 2.97% error rate.

To further demonstrate the validity of the plant height calculation method, the linear correlation of the calculated and

measured plant height was determined for the wheat plant model, as shown in Figure 21.

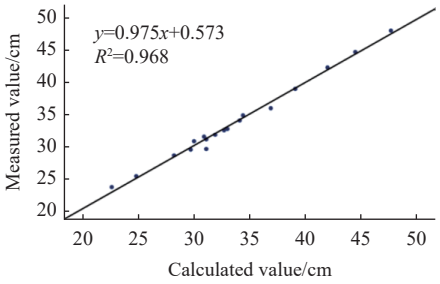

Figure 21 Correlation between calculated and measured values of plant height

Figure 21 shows a high correlation (R^2 = 0.968) between calculated and measured plant heights on the basis of three-dimensional wheat reconstructions. The regression line (slope=0.975, intercept=0.573) confirms strong agreement, validating the three-dimensional reconstruction algorithm's performance.

4.2.2 Leaf length and width calculation and analysis

Because automated leaf segmentation and identification was difficult to achieve, maximum leaf length and width were measured manually using CloudCompare software.

To validate the three-dimensional wheat reconstruction model and the CloudCompare-based method for leaf dimension calculation, the study correlated calculated and measured leaf length and width. The results are shown in Figure 22.

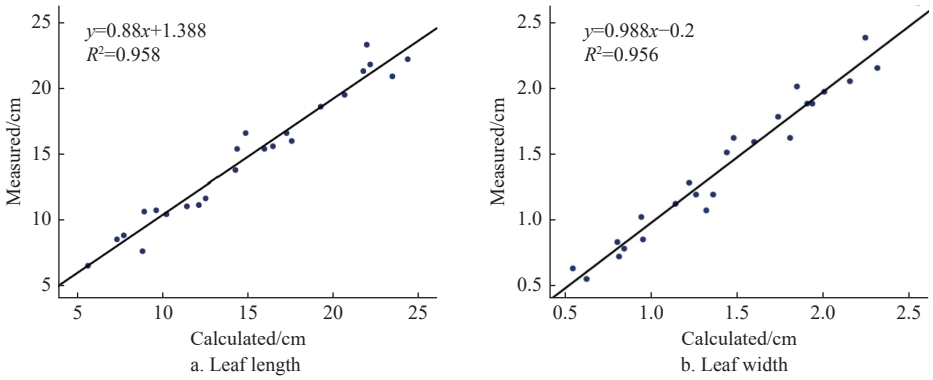

Figure 22 Correlation between calculated and measured values of leaf length and leaf width

For leaf length, the determination-coefficient (R^2) is 0.958, the RMSE is 1.032 cm, the calculation accuracy is 91.28%, and the error rate is 8.72%. For leaf width, the corresponding values are 0.956 (R^2), 0.112 cm (RMSE), 93.66% (accuracy), and 6.34% (error rate).

4.2.3 Calculation and analysis of leaf area and leaf angle

To validate the reliability of the reconstructed wheat three-dimensional model and the greedy triangulation-based leaf area calculation method, the correlation between calculated and measured leaf area values was established. The discrepancy in leaf area estimation is presented in Figure 23.

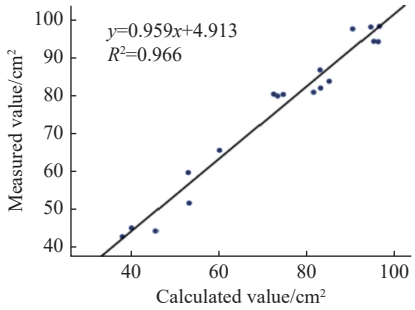

Figure 23 Correlation between calculated and measured values of leaf area

Figure 23 depicts the correlation between calculated and measured leaf areas, yielding an R^2 of 0.966. The fitted regression line exhibits a slope (regression-coefficient) of 0.959 and an intercept of 4.913. The calculation accuracy is 92.80%, with an error rate of 8.2%. The mean absolute error is 3.6132 cm², spanning a range from 1 to 7.2 cm². The calculated value of leaf area is closer to the authentic wheat leaf measurement, which demonstrated the efficiency of three-dimensional reconstruction algorithms of the wheat plant.

To authenticate the credibility of the reconstructed wheat three-dimensional model and the method of calculating leaf angle, a correlation between the calculated values and the measured values of leaf angle was developed. Leaf angle calculation errors derived from the calculated and measured data are shown in Figure 24.

Figure 24 illustrates the correlation between calculated and measured leaf angles, yielding an R^2 value of 0.849. The fitted regression line exhibits a slope (regression-coefficient) of 0.928 and an intercept of 1.647. The error distribution spans from 0.1° to 9.8°, with a mean absolute error of 4.42°. The primary source of error is attributed to the hardware's minimum recognition precision. Moreover, manual measurement had human errors, which would cause some destruction to the wheat leaf structure. On the basis of the reconstructed wheat plant three-dimensional model, wheat leaves and skeletons were extracted. The accuracy rate is 95.17%, and the error rate is 4.83%.

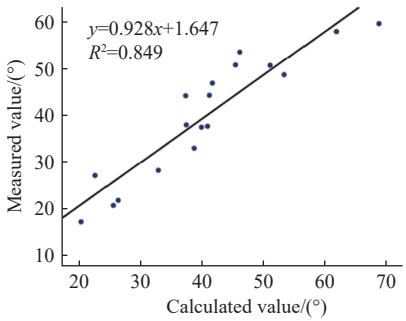

Figure 24 Correlation between calculated and measured values of leaf angle

4.3 Identification and analysis of wheat phenotype

Through the above analysis, it is proven that the reconstructed wheat point cloud model has high accuracy. The phenotypic

information extracted from the wheat model can be directly analyzed and identified.

Therefore, the phenotypes of 36 wheat sample plants were calculated, as shown in Figure 25. At each growth stage, cultivar QM showed the smallest compactness, indicating that the plant configuration of QM was more loose than that of other cultivars and belonged to the loose type. The mean leaf area was estimated based on the number of tillers per plant to enable comparison of tiller phenotypes, as listed in Table 1. QM had the largest average leaf area per plant, and BN had the lowest average plant leaf area on Nov 5, 2022. The results showed that QM had a larger leaf area per plant. Figure 25 indicates that the reconstructed wheat point cloud model is capable of capturing phenotypic differences between cultivars and individual plants.

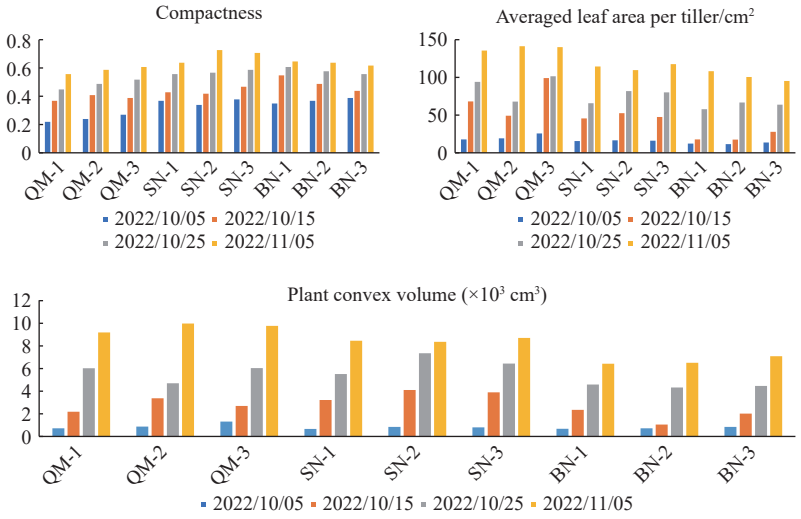

Figure 25 Calculation values of different plant compactness, averaged leaf area per tiller and convex volume

5 Discussion

5.1 Reconstruction strategy

In this study, a multi-perspective method was proposed with a RealSense sensor to achieve the three-dimensional reconstruction of the wheat plant. On the foundation, the phenotype characteristics of wheat plants were accurately calculated.

The three-dimensional reconstruction of wheat plants played a vital role in calculating their phenotypic traits. Due to the reduced presence of noise points in the three-dimensional point cloud data obtained from the multi-view reconstruction system employed, the adopted conditional filtering and SOR filtering methods demonstrated improved effectiveness in achieving target segmentation and data smoothing for individual crop leaves. However, the current method for leaf segmentation in wheat plants only allowed for coarse target extraction, indicating the necessity for further algorithmic refinement and parameter configuration enhancement.

Point cloud overlap with massive unstructured group plants can be used by Rand - LA network and pixel to achieve target detection[34,35]. Lidar extracts plant phenotypes with high accuracy and plays an essential role in agricultural breeding and management[36]. However, it is difficult for lidar to achieve high-speed data acquisition and process it in real time with algorithms. By ensuring accurate phenotype calculation, the point cloud can be streamlined using adaptive curvature-based, downsampling, or random sampling methods to remove redundant data while retaining essential crop information. Subsequently, techniques such as Intrinsic Shape Signatures (ISS), k-dimensional Tree (KD-Tree), and Sample Consensus Initial Alignment (SAC-IA) can be applied during reconstruction to enhance three-dimensional leaf modeling quality and expedite algorithm processing[37–39].

5.2 Experimental design and analysis

This study utilized a multi-view and omnidirectional automated image acquisition device to establish a rapid wheat plant phenotype identification method. Potting experiments for wheat enabled precise control of soil, fertilizer, and water conditions, facilitating study of physiological index trends and development of automated detection methods for challenging metrics like leaf area, leaf angle, and projected area, which are difficult to measure manually. This approach addresses the shortage of mobile wheat phenotyping tools in field or greenhouse settings. Furthermore, the potting method allows for indoor use of large-scale testing equipment, which is also applicable to other field-crops.

There are also some deficiencies in the study. When applying point cloud collection devices with RealSense sensor, due to insufficient light, irregular hetero-colored noise points appeared on the edge of the leaf. Therefore, to boost the detection precision of high-throughput wheat plant phenotypes, it is essential to further refine the data preprocessing algorithm. It is difficult to remove noise with conditional filtering based on color gamut distribution.

In addition, slight vibration will be generated when the turntable drives the plant to rotate, so the image can be acquired after the turntable is stabilized, which increases the reconstruction time.

5.3 Future work

In this work, a high-precision and low-cost multi-perspective three-dimensional reconstruction technology of a wheat plant was proposed based on the Realsense D455 sensor. Data collection, model reconstruction, and phenotypic trait extraction were achieved in a stable indoor environment. Moreover, the physiological indicators that can be measured manually, including plant height, leaf area, and leaf angle, can all be calculated nearly in real time, and good calculation outcomes have been obtained. In future work, a three-dimensional laser scanning platform will be designed for the identification of crop phenotypes by combining multiple laser dot detectors. The platform as a whole is a cube framework, and the module drives multiple laser dot detectors to launch lasers to obtain the depth values of these points, which are used for high-throughput crop point cloud acquisition. Combined with the software we

developed, the automatic segmentation of group crops is realized. It provides a low-cost method for the phenotypic identification of field crops.

In addition to further minimizing the error introduced by the algorithm, we will develop curvature-aware models to better approximate natural leafstalk morphology and optimize point cloud density through adaptive voxel filtering tailored to leafstalk dimensions.

6 Conclusions

Accurately and quickly reconstructing the wheat morphological structure and obtaining wheat traits are the keys to wheat variety selection, scientific cultivation, and precision management. Therefore, a multi-view image acquisition device was designed. The three-dimensional reconstruction of the wheat plant was realized by multi-view acquisition mode, and the nondestructive detection method of wheat phenotypic traits was proposed.

This study utilized conditional filtering and SOR filtering algorithms to reduce noise in wheat plant point cloud data. A combined photometric and geometric objective was optimized, and space positioning was achieved through integration with colored Point Cloud Registration (colored) and Iterative Closest Point (ICP) algorithms. Subsequently, the MVS algorithm was applied to correspond to views using the obtained spatial position, RGB images, and depth images, resulting in the development of a complete wheat plant point cloud model. The algorithm's average reconstruction time is 33.82 s, significantly faster than traditional non-destructive testing algorithms.

Utilizing the reconstructed wheat plant model, the proposed algorithms achieved high accuracy in estimating phenotype characteristics, with plant height, leaf length, leaf width, leaf area, and leaf angle exhibiting accuracies of 97.57%, 91.28%, 93.66%, 92.80%, and 95.17%, respectively. The correlation-coefficients (R^2) with the calculated and measured values for these characteristics were 0.996, 0.958, 0.956, 0.984, and 0.849, indicating a strong positive correlation. These findings demonstrate that the algorithms can accurately and efficiently compute phenotype characteristics. In addition, the phenotypic information of different wheat varieties, such as compactness, convex hull volume, and average leaf area, was analyzed and identified, which proved that the method could capture the phenotypic differences between varieties and individuals. The outcomes of this research are capable of providing technical support and acting as a reference in the realm of growth monitoring. Especially, it could also provide a phenotypic basis for scientific cultivation and good breeding of wheat plant.

Acknowledgements

The authors acknowledge that this work was financially supported by Shandong Provincial Key Research and Development Program (Grant No. 2022LZGCQY002, 2021LZGC013, 2023TZXD004).

[References]

[1] Kaushal S, Gill H S, Billah M M, Khan S N, Halder J, Bernardo A, et al. Enhancing the potential of phenomic and genomic prediction in winter wheat breeding using high-throughput phenotyping and deep learning. Frontiers in Plant Science, 2024; 15: 1410249.

[2] Ren A H, Jiang D, Kang M, Wu J, Xiao F C, Hou P, et al. Evaluation of an intelligent artificial climate chamber for high-throughput crop phenotyping in wheat. Plant Methods, 2022; 18: 1–15.

[3] Spanic V, Lalic Z, Berakovic I, Jukic G, Varnica I. Morphological characterization of 1322 winter wheat (*Triticum aestivum* L.) varieties from EU referent collection. Agriculture, 2024; 14: 551.

[4] Watanabe K, Guo W, Arai K, Takanashi H, Kajiya-Kanegae H, Kobayashi M, et al. High-Throughput phenotyping of sorghum plant height using an unmanned aerial vehicle and its application to genomic prediction modeling. Front Plant Sci, 2017; 8.

[5] Derbyshire M C, Batley J, Edwards D. Use of multiple 'omics techniques to accelerate the breeding of abiotic stress tolerant crops. Current Plant Biology, 2022; 32: 100262.

[6] Xiao Q, Bai X, Zhang C, He Y. Advanced high-throughput plant phenotyping techniques for genome-wide association studies: A review. Journal of Advanced Research, 2022; 35: 215–30.

[7] Wang Y H, Su W H. Convolutional neural networks in computer vision for grain crop phenotyping: A review. Agronomy, 2022; 12: 2659.

[8] Sun D, Robbins K, Morales N, Shu Q, Cen H. Advances in optical phenotyping of cereal crops. Trends in Plant Science 2022; 27: 191–208.

[9] Weyler J, Magistri F, Seitz P, Behley J, Stachniss C. In-Field Phenotyping Based on Crop Leaf and Plant Instance Segmentation, 2022, p. 2725–34.

[10] Tian Y, Zhang J, Zhang Z, Wu J. Research on super-resolution enhancement technology using improved transformer network and 3D reconstruction of wheat grains. IEEE Access 2024; 12: 62882–62898.

[11] Li Y, Wen W, Miao T, Wu S, Yu Z, Wang X, et al. Automatic organ-level point cloud segmentation of maize shoots by integrating high-throughput data acquisition and deep learning. Computers and Electronics in Agriculture, 2022; 193: 106702.

[12] Kargar R A, MacKenzie R, Asner G P, van Aardt J. A density-based approach for leaf area index assessment in a complex forest environment using a terrestrial laser scanner. Remote Sensing, 2019; 11: 1791.

[13] Sun S, Li C, Paterson A H, Jiang Y, Xu R, Robertson J S, et al. In-field high throughput phenotyping and cotton plant growth analysis using LiDAR. Front Plant Sci, 2018; 9.

[14] Zhu R S, Li S, Sun Y Z, Cao Y Y, Sun K, Guo Y X, et al. Research Advances and Prospects of Crop 3D Reconstruction Technology. Smart Agriculture, 2021; 3: 94.

[15] Forero M G, Murcia H F, Méndez D, Betancourt-Lozano J. LiDAR platform for acquisition of 3D plant phenotyping database. Plants, 2022; 11: 2199.

[16] Chen G, Hu L, Luo X, Wang P, He J, Huang P, et al. A review of global precision land-leveling technologies and implements: Current status, challenges and future trends. Computers and Electronics in Agriculture, 2024; 220: 108901.

[17] Pound M P, French A P, Murchie E H, Pridmore T P. Automated recovery of three-dimensional models of plant shoots from multiple color images. Plant Physiology, 2014; 166: 1688–98.

[18] Westoby M J, Brasington J, Glasser N F, Hambrey M J, Reynolds J M. 'Structure-from-Motion' photogrammetry: A low-cost, effective tool for geoscience applications. Geomorphology 2012; 179: 300–314.

[19] Furukawa Y, Hernández C. Multi-view stereo: A Tutorial. CGV, 2015; 9: 1–148.

[20] Wu S, Wen W L, Wang Y J, Fan J C, Wang C Y, Gou W B, et al. MVS-Pheno: A portable and low-cost phenotyping platform for maize shoots using multiview stereo 3D reconstruction. Plant Phenomics, 2020; 2020: 1848437.

[21] Wu S, Wen W, Gou W, Lu X, Zhang W, Zheng C, et al. A miniaturized phenotyping platform for individual plants using multi-view stereo 3D reconstruction. Frontiers in Plant Science, 2022; 13.

[22] Janiszewski M, Prittinen M, Torkan M, Uotinen L. Rapid tunnel scanning using a 360-degree camera and SfM photogrammetry. IOP Conf Ser: Earth Environ Sci, 2023; 1124: 012010.

[23] Ye Z, Bao C, Zhou X, Liu H, Bao H, Zhang G. EC-SfM: Efficient Covisibility-based Structure-from-Motion for both sequential and unordered images. arXivOrg, 2023.

[24] Kang H, Wang X, Chen C. Accurate fruit localisation using high resolution LiDAR-camera fusion and instance segmentation. Computers and Electronics in Agriculture, 2022; 203: 107450.

[25] Wu F, Wang J, Zhou Y, Song X, Ju C, Sun C, et al. Estimation of winter wheat tiller number based on optimization of gradient vegetation characteristics. Remote Sensing, 2022; 14: 1338.

[26] Tadic V, Toth A, Vizvari Z, Klincsik M, Sari Z, Sarcevic P, et al. Perspectives of realsense and ZED depth sensors for robotic vision applications. Machines, 2022; 10: 183.

[27] Vandendaele B, Martin-Ducup O, Fournier R A, Pelletier G, Lejeune P. Mobile laser scanning for estimating tree structural attributes in a temperate

hardwood forest. Remote Sensing, 2022; 14: 4522.

[28] Zou R, Zhang Y, Chen J, Li J, Dai W, Mu S. Density estimation method of mature wheat based on point cloud segmentation and clustering. Computers and Electronics in Agriculture 2023;205: 107626.

[29] Liu R, Chen D, Liu T, Xiong Z, Yuan Z. Learning to predict 3D lane shape and camera pose from a single image via geometry constraints. Proceedings of the AAAI Conference on Artificial Intelligence, 2022; 36: 1765–1772.

[30] Vázquez-Arellano M, Paraforos D S, Reiser D, Garrido-Izard M, Griepentrog H W. Determination of stem position and height of reconstructed maize plants using a time-of-flight camera. Computers and Electronics in Agriculture, 2018; 154: 276–88.

[31] Zhu K, Ma X, Guan H, Feng J, Zhang Z, Yu S. A method of calculating the leafstalk angle of the soybean canopy based on 3D point clouds. International Journal of Remote Sensing, 2021.

[32] Fan Z, Sun N, Qiu Q, Li T, Feng Q, Zhao C. In situ measuring stem diameters of maize crops with a high-throughput phenotyping robot. Remote Sensing, 2022; 14: 1030.

[33] Nair N S, Nair M S. Multi-view stereo using graph cuts-based depth refinement. IEEE Signal Processing Letters, 2022; 29: 1903–1907.

[34] Zine-El-Abidine M, Dutagaci H, Galopin G, Rousseau D. Assigning apples to individual trees in dense orchards using 3D colour point clouds. Biosystems Engineering, 2021; 209: 30–52.

[35] Chen Y, Xiong Y, Zhang B, Zhou J, Zhang Q. 3D point cloud semantic segmentation toward large-scale unstructured agricultural scene classification. Computers and Electronics in Agriculture 2021; 190: 106445.

[36] Jin S, Sun X, Wu F, Su Y, Li Y, Song S, et al. Lidar sheds new light on plant phenomics for plant breeding and management: Recent advances and future prospects. ISPRS Journal of Photogrammetry and Remote Sensing, 2021; 171: 202–23.

[37] Ruchay A, Dorofeev K, Kober A. An efficient detection of local features in depth maps. Applications of Digital Image Processing XLI, vol. 10752, SPIE; 2018; pp.647–654.

[38] Yao Z, Zhao Q, Li X, Bi Q. Point cloud registration algorithm based on curvature feature similarity. Measurement 2021; 177: 109274.

[39] Liang P, Lin W, Luo G, Zhang C. Research of hand–eye system with 3D vision towards flexible assembly application. Electronics, 2022; 11: 354.